PLASIM-GENIE v1.0: a new intermediate complexity AOGCM

P.B. Holden[1], N.R. Edwards[1], K. Fraedrich[2], E. Kirk[3], F. Lunkeit[3] and X. Zhu[4]

[1]Environment, Earth and Ecosystems, The Open University, Walton Hall, Milton Keynes, MK7 6AA, UK

[2]Max Planck Institute of Meteorology, KlimaCampus, Bundesstraße 53, 20146 Hamburg, Germany

[3]Meteorological Institute, University of Hamburg, Bundesstraße 55, 20146 Hamburg, Germany

[4]Center for Earth System Research and Sustainability (CEN), University of Hamburg, Grindelberg 5, 20144 Hamburg, Germany

Abstract

We describe the development, tuning and climate of PLASIM-GENIE, a new intermediate complexity Atmosphere-Ocean Global Climate Model (AOGCM), built by coupling the Planet Simulator to the ocean, sea-ice and land-surface components of the GENIE Earth system model. PLASIM-GENIE supersedes "GENIE-2", a coupling of GENIE to the Reading IGCM. The primitive-equation atmosphere includes chaotic, 3D motion and interactive radiation and clouds, and dominates the computational load compared to the relatively simpler frictional-geostrophic ocean, which neglects momentum advection. The model is most appropriate for long-timescale or large ensemble studies where numerical efficiency is prioritised, but lack of data necessitates an internally consistent, coupled calculation of both oceanic and atmospheric fields. A 1,000-year simulation with PLASIM-GENIE requires approximately two weeks on a single node of a 2.1GHz AMD 6172 CPU. We demonstrate the tractability of PLASIM-GENIE ensembles by deriving a "subjective" tuning of the model with a 50-member ensemble of 1,000-year simulations. The simulated climate is presented considering (i) global fields of seasonal surface air temperature, precipitation, wind, solar and thermal radiation, with comparisons to reanalysis data; (ii) vegetation carbon, soil moisture and aridity index; (iii) sea surface temperature, salinity and the meridional Atlantic and Pacific stream functions. Considering its resolution PLASIM-GENIE

reproduces the main features of the climate system well and demonstrates usefulness for a wide range of applications.

1. Introduction

The Grid-ENabled Integrated Earth system model (GENIE, Lenton et al 2007) has been developed as a modular framework that allows a spectrum of intermediate complexity Earth system models to be created by selecting different options for the various climate and carbon cycle components. Earth system models created within GENIE have been configured for published studies spanning a wide range of geological epochs across Paleozoic, Mesozoic and Cenozoic eras. GENIE framework models are normally capable of integration over multi-millennial timescales and several of the published studies have involved millions of years of simulation time combining long runs and large ensembles. The framework has been designed to be modular to facilitate the coupling of more complex component modules as available computing power increases.

Almost invariably, applications of GENIE have used configurations that represent the atmosphere with a computationally fast energy-moisture-balance-model (EMBM, Fanning and Weaver 1996). These configurations are generically named "GENIE-1". Although adequate for many purposes, especially in the context of global biogeochemical modelling, an EMBM introduces significant structural weaknesses to (or even rules out) a range of applications. Diffusive single-layer moisture transport leads to poor precipitation fields that cannot, for instance, represent convective precipitation or monsoon dynamics. The EMBM applies prescribed surface wind fields (Edwards and Marsh 2005), defined either from climatology or from outputs of more complex models, so that dynamic ocean feedbacks are restricted to the thermohaline circulation. Clouds are represented through a prescribed albedo field (Lenton et al 2006) and a spatially uniform adjustment to outgoing longwave radiation OLR (Holden et al 2010), while uncertain cloud feedbacks on the radiative balance in a changing climate are represented through a globally uniform temperature dependent adjustment to OLR (Matthews and Caldeira 2007, Holden et al 2010).

In an effort to address these shortcomings, the Reading Intermediate General Circulation Model (IGCM3.1, de Forster et al 2000), a 3D dynamical model of the atmosphere, was coupled into GENIE (Annan et al 2005, Lenton et al 2007). Unfortunately this realization of the model "GENIE-2" proved problematic and has only been applied once since these early studies (Holden and Edwards 2010). The coupling with the slab-ocean model was found to exhibit poor precipitation fields, apparently due to structural deficiencies in the convection routine (Annan et al 2005). The coupling with the 3D frictional geostrophic ocean model GOLDSTEIN displays a patchwork-instability and exhibits a low bias in precipitation over ocean. GENIE-2 requires a large moisture flux correction (0.79Sv, reversing the sign of the simulated flux) to reconcile freshwater transport from the Atlantic to the Pacific with reanalysis data (Lenton et al 2007) and generate an Atlantic overturning circulation. A further shortcoming is that, on account of technical complications discussed in Section 3.3, the IGCM was not coupled to the dynamic sea-ice module GOLDSTEINSEAICE, but only to the slab sea-ice module[1].

GENIE-1 has been applied to a wide range of studies, including participation in the EMIC inter-comparisons that were performed for the two most recent IPCC reports (Plattner et al 2008, Zickfeld et al 2013). Although GENIE studies have generally addressed ocean physics, ocean biogeochemistry and the global carbon cycle, a more recent focus has been the development of emulators for climate impact assessment (e.g. Labriet et al 2013, Mercure et al 2014). This application is poorly suited to highly simplified atmospheric models such as the EMBM. Although the emulation techniques were developed from GENIE-2 simulations (Holden and Edwards 2010), this first-generation emulator was not considered sufficiently robust for applications given the poor climatology of the underlying simulator. Instead, a second-generation emulator (Holden et al 2014) was developed using the Planet Simulator PLASIM (Fraedrich 2012).

[1] The GENIE slab sea-ice module assumes a fixed thickness (2m), heat capacity and albedo (0.6). A grid cell becomes completely ice covered when the surface temperature falls below -2°C, with surface temperature evolving according to the energy flux balance. Sea-ice dynamics are neglected and there is no interaction with the hydrological cycle.

PLASIM is a reduced complexity AGCM, with the 3D primitive equation atmosphere model PUMA at its core (Fraedrich et al 2005). We use the PLASIM-ENTS implementation (Holden et al 2014), which incorporates the same land surface model as GENIE. Complementary to GENIE-1, PLASIM has been applied in a range of atmospheric studies, for instance investigating the global entropy budget (Fraedrich and Lunkeit, 2008), double ITCZ dynamics in an aquaplanet (Dahms et al, 2011), the Permian climate (Roscher et al, 2011) and a snowball Earth (Micheels and Montenari, 2008). However, although PLASIM simulates vastly better climatology than the EMBM of GENIE-1, it lacks dynamic representations of ocean and sea ice (and does not model the carbon cycle) so it too neglects important Earth system feedbacks.

We here describe the implementation of a coupling of PLASIM-ENTS to the physical components of the GENIE framework. The coupled model "PLASIM-GENIE" has been developed to join the limited number of models that bridge the gap between EMICS with simplified atmospheric dynamics and state of the art AOGCMs. We are aware of three AOGCMs of comparable complexity with primitive equation atmospheric dynamics: FAMOUS, the reduced resolution implementation of HadCM3, which simulates 1,000 years in approximately ten days on eight CPUs (Williams et al, 2013), SPEEDO, comprising a T30 spectral atmosphere with simplified parameterizations (Molteni 2003) coupled to a primitive equation ocean model, which simulates 1,000 years in approximately two weeks on a 3GHz dual core Intel E6850 CPU (Severijns and Hazeleger, 2010) and OSUVic, a coupling of PLASIM to the UVic Earth system model (Schmittner et al, 2010). A 1,000-year simulation with PLASIM-GENIE requires approximately two weeks on a single node of a 2.1GHz AMD 6172 CPU.

State of the art climate models operate at the limit of available computing power, so that very few simulations can be performed with these models. An important motivation for intermediate complexity models is for the evaluation of uncertainty. We here demonstrate the tractability of PLASIM-GENIE ensembles by tuning the model with a 50-member ensemble of 1,000-year simulations.

2. Component Modules

2.1 PLASIM-ENTS

PLASIM (Fraedrich 2012) is a reduced complexity AGCM, with the 3D primitive equation atmosphere model PUMA at its core (Fraedrich et al 2005). PLASIM is described in detail in Lunkeit et al (2007) and references therein. We summarise briefly here. The atmospheric dynamics are solved using the spectral transform method, formulated for temperature, specific humidity, log surface pressure, divergence and vorticity. The short wave radiation scheme separates solar radiation into two bands, $\lambda < 0.75\mu m$ (with cloud scattering, ozone absorption and Rayleigh scattering) and $\lambda > 0.75\mu m$ (with cloud scattering, cloud absorption and water vapour absorption). The long wave radiation scheme uses the broad band emissivity method, with the (greenhouse gas) effect of water vapour, carbon dioxide and ozone included in the calculation of emissivity. Ozone concentration is prescribed with an analytic spatio-temporal distribution. Cloud emissivity is calculated from the cloud liquid water content. Fractional cloud cover is diagnosed from relative humidity (stratiform clouds) and from the convective precipitation rate (convective clouds). Other parameterised processes include large-scale precipitation, moist convection (both cumulus and shallow), dry convection, boundary layer heat fluxes, vertical diffusion (to represent unresolved turbulent exchange) and horizontal diffusion (applied to selectively dampen short wavelengths in spectral space).

The land surface scheme (previously the "Simulator for Biospheric Aspects" SimBA, Kleidon et al 2005) was modified (Holden at al 2014) to use GENIE's "efficient numerical terrestrial scheme" ENTS (Williamson et al 2006), partly in anticipation of this coupling to GENIE. ENTS models vegetative and soil carbon densities, assuming a single plant functional type that has a doubled-peaked temperature response (representing boreal and tropical forest). In addition to temperature, the rate of photosynthesis depends upon the atmospheric CO_2 concentration and on soil moisture availability. ENTS includes a parameterisation of self-shading, so that new photosynthetic production is channelled into leaf litter when fractional vegetation coverage approaches one and the canopy closes. Land surface albedo, moisture bucket

capacity and surface roughness are parameterised in terms of the simulated carbon pool densities. We note that although the state variables simulated by ENTS are the vegetation and soil carbon densities, we have not coupled PLASIM-GENIE to the GENIE-1 carbon cycle; this extension is straightforward in principle and will be addressed in future work. In this coupling, ENTS can be run in a diagnostic mode (setting parameter *nbiome*=2), simulating dynamically changing terrestrial carbon pools without affecting the climate state.

PLASIM includes flux-corrected slab ocean and sea-ice models[2]. The coupling described here (Section 3) replaces these simple models with the 3D dynamical ocean model GOLDSTEIN and the thermodynamic-dynamical sea ice model GOLDSTEINSEAICE.

2.2 GOLDSTEIN

GOLDSTEIN is a 3D frictional-geostrophic ocean model (Edwards and Marsh, 2005; Marsh et al, 2011). GOLDSTEIN is dynamically similar to classical GCMs, except that it neglects momentum advection and acceleration. Barotropic flow around Antarctica is derived from linear constraints that arise from integrating the depth-averaged momentum equations; we here neglect flow through other straits. Several modifications to the default GOLDSTEIN can be enabled; here we apply the modified equation of state that includes a density adjustment for thermobaricity given by $2.5\times10^{-5}Tz$ kgm^{-3}, where T is temperature (°C) and z is height i.e. negative depth (m), and the enhanced diapycnal mixing scheme (Oliver and Edwards, 2008).

2.3 GOLDSTEIN SEA ICE

GOLDSTEINSEAICE (Edwards and Marsh, 2005) solves for the fraction of the ocean surface covered by ice within a grid cell and for the average sea-ice height. A diagnostic equation is solved for the ice surface temperature. Growth or decay of sea ice depends on the net heat flux into the ice (Semtner, 1976; Hibler 1979);

[2] The PLASIM sea-ice model is based on the thermodynamic model of Semtner (1976). It neglects dynamics. Spatio-temporal energy flux corrections are diagnosed from comparison with observed present-day sea-ice thickness.

sea-ice dynamics consists of advection by surface currents and diffusion. The thermodynamics of GOLDSTEINSEAICE are summarized in detail in Section 3.3.

3. Coupling methodology

A schematic of the PLASIM-ENTS/GOLDSTEIN/GOLDSTEINSEAICE 'pl_go_gs' coupling is illustrated in Figure 1.

In order to avoid the need for interpolation, the coupling was set up to require the three models have matched horizontal grids. PLASIM has previously been configured for T21, T31 and T42 resolutions. Here we restrict the coupling to T21 and use the matched 64x32 GOLDSTEIN grid (Lenton et al 2007). PLASIM vertical resolution is 10 levels. GOLDSTEIN depth resolution is 32 levels, with bathymetry defined at the resolution of the 8 level configuration. Extension to other resolutions (horizontal or vertical) is straightforward in principle.

The computational demands of the coupled model, simulating 75 years per day on a single node of a 256Gb 2.1GHz AMD 6172 CPU, are dominated by PLASIM (98%). The computational demands of PLASIM are dominated by diabatic processes (~76%), in particular by radiation (~43%) and precipitation (~16%). We note that the modular structure of PLASIM means that replacing the radiation scheme with, for example, a computationally fast semi-grey scheme (Frierson et al 2006) would be relatively straightforward. An efficient convective adjustment scheme (Betts and Miller 1986) is already available as an alternative to the default moisture budget scheme (Kuo 1965, 1974).

3.1 PLASIM-ENTS

The choice was made to preserve the coupled PLASIM-ENTS model in its entirety. The slab ocean and sea ice modules are retained only to provide boundary conditions; their state variables are over-written with GOLDSTEIN and GOLDSTEINSEAICE outputs, effectively negating the very simple dynamics of these models. This simplifies the coupling because the energy and moisture flux calculations are already made within PLASIM. The changes needed to PLASIM with this approach are therefore kept to a minimum, consisting of prescribing the slab ocean with

GOLDSTEIN distributions of sea surface temperature and the slab sea-ice with GOLDSTEINSEAICE distributions of sea-ice fractional coverage, height, surface temperature and albedo. Furthermore, although GENIE contains a stand-alone version of the land surface module ENTS, the decision was taken to leave the existing PLASIM-ENTS coupling in place. Future work may separate the PLASIM and ENTS modules. The primary motivation for this would be modularity. Notably GENIEfied ENTS is coupled to the global carbon cycle (Lenton et al 2006) and has been enabled to simulate the effects of anthropogenic land use change (Holden et al 2013a).

3.2 GOLDSTEIN

No changes were made to GOLDSTEIN. Surface wind stress, net energy and net moisture fluxes are supplied from PLASIM, modified by sea ice where relevant. We note that we use a PLASIM time step of 45 minutes and a GOLDSTEIN time step of 12 hours, with coupling inputs averaged over the previous 16 PLASIM time steps (12 hours.

3.3 GOLDSTEINSEAICE

In GENIE-1 the thermodynamics of GOLDSTEINSEAICE are calculated within the EMBM, and coupling to alternative model atmospheres is not possible with this model structure. To enable a PLASIM-GOLDSTEINSEAICE coupling we have developed a stand-alone sea-ice thermodynamics routine.

Time-averaged incoming energy fluxes and atmospheric boundary conditions are supplied to the new surface flux (ICE-SURFLUX) routine from PLASIM. Sea surface temperature and salinity, sea-ice height and fractional sea-ice coverage are provided from the previous GOLDSTEIN/SEAICE time step.

ICE-SURFLUX closely follows the formulation of Edwards and Marsh (2005), where it is described in some detail. We summarize the approach here. Sea ice is assumed to have no heat capacity, so that the heat flux exchanged with the atmosphere equals the heat flux through the ice, thereby defining the vertical temperature gradient across the ice. The temperature at the sea-ice base is assumed equal to the salinity-dependent freezing point of the surface ocean, so

that the ice-surface temperature is the remaining unknown. Now we need to derive the net heat flux from the atmosphere. Incoming radiative fluxes are provided by PLASIM; outgoing radiative fluxes, and sensible and latent heat fluxes are dependent upon the surface temperature of the sea ice, together with atmospheric boundary conditions. These relationships together imply an ice-surface temperature (and the associated atmospheric heat flux) that balances the heat budget, which is solved for with a Newton-Raphson algorithm. The heat flux exchanged with the ocean is implied by the temperature differential between the sea-ice base (freezing point) and the surface ocean. The difference between the heat flux exchanged with the atmosphere and with the ocean is consumed by creating or melting ice.

The diagnosed energy and moisture fluxes are not passed to PLASIM. Instead, in order to achieve energy and moisture conservation, PLASIM transfer coefficients are used in the calculation of sensible heat and sublimation during the Newton-Raphson step. This ensures that net fluxes calculated in PLASIM (which use the sea-ice temperature and albedo derived in ICE-SURFLUX) will be consistent with those calculated in ICE-SURFLUX, but does not guarantee perfect conservation. Conservation errors arise through differential time-stepping (the averaging of non-linear flux terms over 16 PLASIM time steps) and also because PLASIM does not explicitly account for sea-ice leads; ICE-SURFLUX separately accounts for ocean and sea-ice in a partially covered gridcell, but PLASIM fluxes are derived from weighted average surface properties[3]. To evaluate the magnitude of the conservation errors, we consider all of the sea-ice covered grid cells at each time step across a year of the spun-up model. The energy conservation error across these 152,495 data points is $0.1 \pm 1.0 \mathrm{Wm}^{-2}$ (1σ). We note that the PLASIM atmosphere does not precisely conserve energy, as illustrated by Hoskins and Simmons (1975) for a similar dry dynamical core. The largest effect in PLASIM

[3] A drift over the 2,000-year spin-up simulation is apparent in the 6th significant figure of global averaged salinity, likely also a consequence of the neglect of sea-ice leads in PLASIM and the differential time-stepping. While this modest failure of moisture conservation is negligible for the physical model, it will be revisited for the carbon cycle coupling in order to ensure conservation of biogeochemical tracers.

comes from the conversion from potential to kinetic energy. This conversion cannot be formulated in a conservative manner in the semi-spectral scheme since it involves triple products while the (Gaussian) grid only allows for the conservation of quadratic quantities. The top-of-atmosphere energy balance converges to -0.7Wm^{-2} in both the coupled and stand-alone versions of PLASIM, dominating over the conservation errors of ICE-SURFLUX.

Sea-ice growth rates are provided to GOLDSTEINSEAICE, which derives updated sea-ice distributions, considering both thermodynamics and dynamics (advection and diffusion). The updated sea-ice distribution is provided to PLASIM and the associated freshwater exchange with the ocean is provided to GOLDSTEIN.

4. Tuning methodology

Our approach for the selection of a tuned set of parameter values was to retain the existing tunings of models where possible (for exceptions see Section 4.1) and to only consider the parametric uncertainty of GOLDSTEIN. The motivation was that both PLASIM (Lunkeit et al 2007) and ENTS (Williamson et al 2006) have already been tuned to reproduce observations when forced with climatology[4]. In contrast, existing GOLDSTEIN tunings have been developed within a coupled atmosphere-ocean model, usually the EMBM atmosphere. We anticipated that a tuning of GOLDSTEIN that reproduces the main features of global ocean circulation when coupled to climatologically tuned PLASIM-ENTS would likely provide a good representation of observed climatology in general.

We performed a 50-member ensemble of 1,000-year preindustrial spin-up simulations varying six GOLDSTEIN parameters, in the expectation that some subset of ensemble members would produce reasonable climate states from which we could select a tuned model. (Failure in this regard would have necessitated the application of more sophisticated statistical techniques for searching parameter input space).

316

317 **4.1 Ensemble design**

318 Parameters from modules other than GOLDSTEIN were all fixed. However, some
319 were changed from their default values (or are recently introduced
320 parameterisations that are not associated with tuned defaults). These choices
321 were made on the basis of exploratory simulations:

322 i) The uncertain effect of clouds on long wave radiation is controlled
323 through the dependence of cloud emissivity A on the mass absorption
324 factor k "acllwr", following Slingo and Slingo (1991):

$$A = 1 - e^{-\beta k W}$$

325 where $\beta = 1.66$ is the diffusivity factor and W the cloud liquid water
326 path. The mass absorption factor was found to exert the strongest
327 control on surface air temperature of the 22 key model parameters
328 considered in PLASIM-ENTS ensembles (Holden et al 2014). The value
329 was increased from default $k = 0.1$ to $0.2 m^2 g^{-1}$, estimated to yield a
330 simulated global average surface air temperature of approximately
331 14°C in conjunction with parameter choices (ii) to (v) below.

332 ii) The PLASIM parameter *albseamax* defines the latitudinal variation of
333 ocean albedo (Holden et al 2014),

$$\alpha_s = \alpha_{s0} + 0.5\alpha_{s1}[1 - cos(2\varphi)]$$

334 where the ocean albedo α_s is expressed in terms of latitude φ, the albedo
335 at the equator $\alpha_{s0} = 0.069$ and the parameter that controls latitudinal
336 variability α_{s1}. The calculated albedo is applied to both direct and
337 scattered radiation. A high value ($\alpha_{s1} = 0.4$) was favoured for
338 *albseamax*, leading to cooler high latitude ocean and favouring
339 increased Southern Ocean sea-ice and deep-water formation, which
340 both tended to be too low with default parameters.

341 iii) Sea ice is transported through advection and Laplacian diffusion
342 (Edwards and Marsh, 2005), the latter taking the place of a detailed
343 representation of unresolved advection and rheological processes.
344 Sea-ice diffusivity (*SID*) influences AABW formation by controlling the

---

[4] The diurnal cycle is switched off in these simulations, reflecting the default

rate at which new ice is created, and hence the strength of brine rejection (Holden et al 2013b). A high value was favoured, again to strengthen deep-water formation, but values greater that 15,000 m^2s^{-1} were found to lead to numerical instabilities in this model and *SID* was fixed at this value.

iv) The standard PLASIM expression for the dependence of sea ice albedo α_i on surface air temperature is used

$$\alpha_i = 0.5 - 0.025T_{air}$$

where T_{air} is the surface air temperature (°C). PLASIM restricts the maximum albedo to 0.7 ($T_{air} \leq -8$°C). In PLASIM-GENIE we additionally restrict the minimum albedo, to 0.5 ($T_{air} \geq 0$°C).

v) The PLASIM-ENTS dependency of photosynthesis on soil moisture is

$$f_2(W_s) = \{(W_s/W_s^*) - q_{th}\}/\{0.75 - q_{th}\}$$

The parameter q_{th} (*qthresh)* was set to 0.1, allowing the development of vegetation in semi-arid regions (Holden et al 2014).

The ensemble was generated using a 50x6 maximin latin hypercube design, varying six GOLDSTEIN parameters, listed in Table 1 and varied over ranges considered to reflect the plausible range for each parameter (Holden et al 2013b and references therein). The six varied parameters are isopycnal and diapycnal diffusivities, a parameter *OP1* that controls the depth profile of diapycnal diffusivity (see below), the frictional drag coefficient (GOLDSTEIN is based upon the thermocline equations with the addition of a linear drag term in the horizontal momentum equations, Edwards et al 1998), wind stress scaling (a linear scaling of the surface wind-stress is applied to compensate for the energy dissipated by frictional drag), and an Atlantic-Pacific moisture flux adjustment.

Diapycnal diffusivity is stratification-dependent (Oliver and Edwards, 2008), given by

$$k_v = k_{v0} p_0(z)^\gamma \left(\frac{\Delta\rho_0(z)}{\Delta\rho(z)} \right)$$

---

assumption for both the PLASIM and ENTS tunings.

where k_{v0} (reference diapycnal diffusivity) and γ ($OP1$) are varied across the ensemble (Table 1), $p_0(z)$ is a reference profile (exponentially growing with depth and equal to 1 at 2500m), $\Delta\rho_0(z)$ a reference vertical density gradient profile and $\Delta\rho(z)$ the local simulated vertical density gradient.

Two ensemble parameters merit particular discussion here:

4.1.1 APM

APM is a flux adjustment that transports moisture from the Atlantic to the Pacific, originally developed for the EMBM coupling (Edwards and Marsh, 2005). The default flux adjustment (0.32Sv) is subdivided into three latitude bands reflecting the observed Atlantic-Pacific moisture transport (Oort, 1983): -0.03Sv south of 20°S, 0.17Sv in the tropical zone 20°S to 24°N, and 0.18Sv north of 24°N. Exploratory simulations suggested that PLASIM-GENIE would likely require a moisture flux adjustment and *APM* was introduced as an ensemble variable. *APM* is varied across ensemble members by a linear scaling preserving the ratio of fluxes between latitude bands.

An exploratory simulation with a flux adjustment of 0.32Sv was performed and integrated net input freshwater fluxes (precipitation, evaporation, runoff and the flux adjustment) were diagnosed for the Arctic/Atlantic and the Pacific. In both basins, grid cells north of 32°S were included, following the observational estimates of Talley (2008). Values of -0.5Sv and +0.1Sv respectively were diagnosed, compared to observations of -0.28±0.04 and +0.04 ± 0.09Sv (Talley 2008). Informed by this result, we allowed *APM* to vary in the range 0 to 0.32Sv.

PLASIM has also been coupled to the UVic Earth system model, creating the OSUVic model (Schmittner et al, 2010). The most significant difference between PLASIM-GENIE and USOVic is the differing complexity of the ocean models; USO-Vic incorporates the more complex primitive-equation Modular Ocean Model (MOM) version 2.2 (Pacanowski 1995) at a horizontal resolution of 1.8° x 3.6°. The primitive equations include momentum advection terms neglected in our system. At T21 atmospheric resolution, the integrated Atlantic surface moisture

balance simulated by OSUVic (-0.33Sv) is in good agreement with observations without any flux adjustment. However, OSUVic nevertheless simulates a weak (9Sv) Atlantic overturning circulation at T21 resolution. This was attributed in part to errors in the latitudinal distribution of the simulated moisture flux, which create low surface ocean salinities at high latitudes in the Atlantic (balanced by high salinity at low latitudes). We note that an exploratory PLASIM-GENIE simulation with a *uniformly* distributed 0.32Sv moisture flux adjustment also exhibited low Atlantic salinity at high latitudes and weak overturning.

4.1.2 SCF

SCF scales the surface wind stresses that are applied to GOLDSTEIN. The scaling is needed because the frictional-geostrophic ocean dissipates wind energy so that increased surface wind strengths are required to compensate and drive a reasonable circulation. The conventional ensemble range for the *SCF* parameter in GENIE-1 (forced by observed climatological wind stress) is 1 to 3 (Edwards and Marsh, 2005).

In the OSUVic model (Schmittner et al 2010), the weak overturning circulation at T21 resolution discussed in Section 4.1.1 was, in addition to errors in the surface salinity distribution, partly attributed to low zonal wind-stress in the Southern Ocean, likely due to inadequate meridional resolution (c.f. Held and Phillipps, 1993). In anticipation of systematically understated Southern Ocean zonal wind stress in our T21 coupling, we here allowed *SCF* to vary in the range 2 to 4.

4.2 Ensemble outputs

Thirty-seven of the 50 ensemble members successfully completed the 1,000-year preindustrial spin up simulations. These simulations exhibited a global average surface air temperature of 12.1±1.2°C (1σ). Simulation-failure was invariably associated with low frictional drag (high *ADRAG*); low frictional drag leads to unrealistically strong flow near the Equator and topographic features (Edwards and Marsh, 2005). Three successfully completed simulations (with inverse frictional drag 4.01, 3.21 and 3.98 $days^{-1}$) were excluded from the ensemble on account of unreasonably strong Pacific overturning (277, -174 and 633Sv

438 respectively). We briefly summarise some of the characteristics of the remaining
439 thirty-four simulations in terms of their response to *APM*, *SCF* and *ADRAG*, the
440 three parameters that dominate the ensemble variability.
441
442 **4.2.1 APM**
443 The Atlantic overturning cell collapsed in all 20 simulations with *APM* less than
444 0.16Sv. It collapsed in only five of the 14 simulations with *APM* greater than
445 0.16Sv.
446
447 A regression of ensemble outputs suggests that the observed integrated Atlantic
448 freshwater balance (correlation -0.88) is best reproduced for *APM* of
449 approximately 0.13Sv, while the integrated Pacific freshwater balance
450 (correlation +0.57) is best reproduced for *APM* of approximately 0.28Sv. Values
451 between these limits (~0.13 to 0.28Sv) are therefore favoured to optimise the
452 surface ocean inter-basin salinity distribution.
453
454 It is worth noting that these conclusions only pertain to the specific model setup
455 considered (i.e. the vector of all *fixed* parameters). We cannot rule out the
456 possibility that alternative model parameterisations can reproduce observed
457 salinity and circulation fields without a moisture flux adjustment.
458
459 **4.2.2 SCF and ADRAG**: Wind stress scaling and inverse frictional drag affect the
460 simulations in similar ways, as expected because the role of wind-stress scaling
461 is to compensate for frictional dissipation. Many clear relationships between
462 these parameters and simulated outputs are apparent, for instance high values of
463 either tend to strengthen overturning circulation and decrease sea-ice coverage
464 in both hemispheres. It is interesting to note a strong negative correlation (-0.62)
465 between *ADRAG* and the integrated surface Pacific freshwater flux, opposing a
466 positive correlation (+0.77) with the integrated freshwater flux of the Indian
467 Ocean. (Similar, though weaker, relationships exist with *SCF*).
468
469 **4.3 Selection of a 'subjectively' tuned parameter set**

Three of the 37 completed 1,000-year simulations have already been ruled out for unreasonably strong Pacific overturning and a further twenty-five because the Atlantic overturning circulation had collapsed. Two further simulations were ruled out for unacceptably low (and still cooling) global surface air temperature (<10°C) and two for an excessively evaporative Atlantic basin (~0.5Sv, forced by *APM* ~0.3Sv). The remaining five simulations were spun on for an additional 1,000 years. After this spin on, two of these simulations were ruled out under a stricter global surface air temperature constraint (requiring >12°C), a third simulation did not exhibit penetration of Antarctic Bottom Water into the Atlantic and a fourth simulation displayed a positive Pacific overturning cell that penetrated to the ocean floor north of 15°N. The remaining simulation was clearly preferable on the basis of these simple large-scale constraints, testing for reasonable surface-ocean forcing and circulation. This 'subjective' parameter set (see Table 1) is therefore taken as our preferred tuning[5].

5.0 Simulated climate of the subjective tuning

The simulated climate metrics of the subjective tuning are global average surface air temperature 12.9°C, surface Atlantic freshwater balance -0.34Sv (including the -0.21Sv moisture flux adjustment), maximum Atlantic overturning (below 500m) 15.5Sv, minimum Atlantic overturning -3.4Sv, and maximum Pacific overturning 8.8Sv (restricted to high latitudes and intermediate depths, see Figure 6). We now evaluate the climate in some detail.

Table 2 compares the subjectively tuned PLASIM-ENTS preindustrial global energy balance against a range of observationally constrained (present day) estimates presented in Trenberth et al (2009). Simulated fluxes are generally within the ranges of these estimates besides reflecting the simulated cold bias that is most clearly apparent in OLR (and only partially attributable to

[5] We note that after the tuning ensemble was performed, the "surfstep" PLASIM subroutine was moved to the start of the diabatic time step (in the stand-alone model, PLASIM surface conditions are updated after the calculation of diabatic processes). This change was made so that boundary conditions are immediately updated after a call to GOLDSTEIN. Differences in simulated outputs were not distinguishable from internal variability.

anthropogenic forcing). Although within ranges, these data suggest that too little solar radiation is absorbed within the atmosphere and too much is reflected by the surface (likely due to the high ocean albedo, Section 4.1).

Table 3 compares the simulated surface ocean net moisture fluxes in each basin with the estimates of Talley (2008). The good agreement in the Atlantic is imposed by the moisture flux adjustment. We emphasise that the requirement for a flux adjustment in this parameterisation does not necessarily indicate an inherent structural weakness in the model, pending a full exploration of parameter-space (c.f. Williamson et al 2015). The largest disagreement between these observations and the subjective tuning is the moisture flux differential between the Indian and Pacific Oceans. The global aggregates of precipitation, evaporation and runoff are in good agreement with the observationally constrained estimates of Trenberth et al (2007), with a modest low bias that is consistent with the simulated cold bias.

Figures 2 to 4 compare a selection of PLASIM-GENIE outputs against NCEP/NCAR reanalysis fields (Kalnay et al 1996). In each case we compare fifty-year PLASIM-GENIE averages of southern summer (JJA) and northern summer (DJF) with the corresponding long-term means (1981-2010) of the reanalysis data. The plotted outputs were chosen to highlight feedbacks that are neglected by the EMBM, viz. 3D dynamical atmospheric transport, providing greatly improved precipitation fields and dynamic surface winds (an imposed forcing in GENIE-1), and interactive clouds (also an imposed forcing field in GENIE-1, comprising a spatiotemporal cloud albedo field and uniform OLR adjustment.)

Surface air temperature and precipitation fields are plotted in Figure 2. The cold bias of the subjective tuning is especially apparent in the high Arctic winter. Despite the global cold bias, surface air temperatures are warm-biased over the Southern Ocean, consistent with an underestimation of southern sea-ice coverage that was apparent over the entire ensemble. PLASIM precipitation fields are reasonable given our low resolution. Distinct arid regions are captured,

530 as is the seasonal migration of the Inter-Tropical Convergence Zone and
531 associated monsoon systems.
532
533 Figure 3 compares the surface wind fields of the subjective tuning with 10m
534 reanalysis winds. The simulated spatiotemporal distributions are in good
535 agreement with reanalysis, although Antarctic circumpolar wind speed is
536 somewhat understated and too northerly (c.f. Schmittner et al 2010). We note
537 that simulated wind speeds are at the 0.983 sigma pressure level, typically
538 ~136m above the surface, so that boundary layer damping is weaker than the
539 10m reanalysis winds. Therefore we expect greater wind speeds in the PLASIM-
540 GENIE plots, as is generally the case. Our focus here is on the wind-stress
541 coupling and the tuned ocean state. The 3D atmospheric circulation is also
542 reasonable. To illustrate, the simulated Southern/Northern hemisphere winter
543 zonal wind jets (~44/43 ms^{-1}, 35°S/35°N, 150mbar) compare to reanalysis data
544 (~41/44 ms^{-1}, 30°S/30°N, 200mbar).
545
546 Figure 4 compares incoming solar and thermal radiation fields with the
547 reanalysis data. These fields are also chosen to reflect dynamics that are absent
548 from GENIE-1, which applies prescribed planetary albedo fields and a globally
549 uniform OLR adjustment to represent the effect of clouds on the radiation
550 balance. The outputs plotted in Figures 3 and 4 were chosen to focus on
551 dynamics that are entirely absent from GENIE-1: interactive winds and
552 interactive clouds. While the inclusion of these dynamics is not expected to
553 improve the simulated climatology (i.e. when compared to simulations that are
554 forced with climatological fields), their inclusion represents a substantial
555 upgrade through the capture of important Earth system feedbacks neglected in
556 GENIE-1.
557
558 An important example of substantial improvement over the climatology of
559 GENIE-1 is atmospheric moisture transport, previously touched upon in the
560 context of Figure 2. Figure 5 compares PLASIM-GENIE vegetative carbon (5a)
561 and GENIE-1 vegetation carbon (5b, data reproduced from Holden et al, 2013a,
562 Fig 1a) and highlights various aspects of the improved moisture transport. In

GENIE-1, deserts are poorly resolved (too moist) and boreal forest does not penetrate far into the continental interior of Eurasia (too dry); these are both shortcomings that arise from diffusive moisture transport (Lenton et al 2006). Although the deserts of the Southern hemisphere are not well resolved in either model, the larger deserts of the Northern hemisphere are distinct in PLASIM-GENIE, while simulated boreal forest penetrates the Eurasian interior. Global terrestrial carbon storage in the subjective tuning of PLASIM-GENIE is 604GTC (vegetation) and 1,971GTC (soil). These compare to 491-574 GTC and 1,367-1,416GTC respectively in GENIE-1 (Lenton et al 2006). The significantly higher soil carbon values in PLASIM-GENIE primarily reflect the increased area of Eurasian boreal forest, where soil carbon is respired slowly due to the low temperatures. The global terrestrial carbon pools are consistent with ranges of 460-660GTC (vegetation) and 850-2400GTC (soil) derived from a range of observational and modelling studies and summarised in Bondeau et al (2007).

Budyko's (1974) framework of climate analysis is based on the climate mean dryness ratio D or aridity index (mean energy supply or net radiation N to mean water supply or precipitation P). It provides quantitative geobotanically relevant thresholds for land surface climate regimes that are related to vegetation structures (Fig. 6c): Tundra, $D < 1/3$, and forests, $1/3 < D < 1$, are energy limited ($D < 1$), because available energy N is low, so that runoff exceeds evaporation for given precipitation, $E \sim N$. Steppe and savanna, $1 < D < 2$; semi-desert, $2 < D < 3$; and desert $3 > D$, are water-limited climates ($D > 1$), where the available energy is so high that water supplied by precipitation evaporates, which then exceeds runoff, $E - P$. This analysis highlights the Tibetan Plateau and North American Arctic climates and demonstrates consistency with the simulated vegetation carbon (Fig 6a). The similarity with ERA-interim based analysis (Cai et al 2014, Fig 1a) is notable. Similarly, a bucket model interpretation of the land surface climate (Fraedrich et al 2015) is possible using the soil moisture fraction, $S=s/s^*=E/N$, and is plotted in Fig. 5d.

Sea-ice distributions (not illustrated) exhibit a systematic bias towards low southern sea-ice area across the ensemble, with an annual average of 2.8 million

596 km^2 in the subjective tuning; this compares to observational estimates of 11.5
597 million km^2 (Cavalieri et al 2003). Surface air temperature over the southern
598 ocean is warm biased with respect to the reanalysis data, despite a modest cold
599 bias in the global temperature (Figure 2). While this may in part be a
600 consequence of reduced sea-ice (through the albedo feedback), the continued
601 presence of the warm bias in southern summer suggests the possibility that the
602 bias arises in the atmosphere. The decision to control the global temperature
603 with *acllwr* (Section 4.1) preferentially warms cloudy regions and may have
604 contributed. Indeed, simulated downward thermal radiation exhibits a
605 significant bias over the Southern Ocean (Figure 4). A thorough investigation of
606 the source of this bias is beyond the scope of this study, requiring consideration
607 of uncertainties in atmospheric and ocean energy transport, and in solar and
608 thermal radiative transfer, considering clouds, water vapour, and surface
609 processes.
610
611 Figure 6 illustrates aspects of the simulated ocean state that directly reflect the
612 constraints imposed upon the subjective parameter set and require little further
613 discussion. It is worth emphasising again that the simulation of realistic salinity
614 fields and ocean circulation required an Atlantic-Pacific moisture flux adjustment
615 in this parameterisation (Sections 4.1.1 and 4.2.1).
616
617 The upper panel of Figure 7 plots the PLASIM-GENIE barotropic streamfunction.
618 Simulated gyre strengths are 24Sv/-26Sv North/South Atlantic, 53Sv/-41Sv
619 North/South Pacific and 5Sv/-32Sv North/South Indian Ocean. For comparison,
620 the gyre strengths of climatological wind-forced 64x32 GENIE-1 were simulated
621 at ~20Sv/-20Sv North/South Atlantic, ~30Sv/-30Sv North/South Pacific and
622 ~3Sv/-40Sv North/South Indian Ocean at (Figure 19d, Marsh et al 2011).
623 Stronger gyres in the PLASIM-GENIE simulation compared to the GENIE-1
624 simulation are likely to be related to larger values of wind-stress scaling in the
625 PLASIM-GENIE case, given that the simulated wind forcing is relatively close to
626 climatology. The observed Gulf Stream strength is estimated at 32Sv, while
627 simulated strengths ranged from 13 to 48Sv in the multi-model comparison of
628 Balan-Sarojini et al (2011). The Antarctic Circumpolar Current (ACC) is weaker

in PLASIM-GENIE (30Sv) than GENIE-1 (47Sv), presumably reflecting the weak simulated Southern Ocean zonal winds (see Figure 3). Note that both models significantly understate the ACC strength compared to observations of 140±6Sv (Ganachaud and Wunsch, 2000).

The lower panel of Figure 7 illustrates high-frequency AMOC variability driven by atmospheric dynamics, behaviour that is absent from GENIE-1 (Balan-Sarojini et al 2011). The maximum Atlantic overturning circulation is plotted through an arbitrary year (year 100 of a spin on simulation), together with the 100-year mean and standard deviation.

6.0 Summary and conclusions

We have presented a new intermediate complexity AOGCM PLASIM-GENIE, which reproduces the main features of the climate system well and represents a substantial upgrade to GENIE-1 through the representation of important atmospheric dynamical feedbacks that are absent in an EMBM. PLASIM-GENIE has been developed to join the limited number of intermediate complexity models with primitive equation atmospheric dynamics. It supersedes an earlier coupling with the IGCM ('GENIE-2'), which was contaminated with spurious numerically generated features, limiting its usefulness.

The simple 'subjective' tuning approach applied here considered only six ocean parameters, seeking a reasonable ocean circulation when coupled to PLASIM-ENTS (both PLASIM and ENTS have previously been tuned with climatological forcing). This limited tuning approach required approximately 2 CPU years, demanding but readily tractable, representing approximately two weeks of computation on 50 cluster nodes.

A reasonable ocean circulation state and salinity distribution required the application of an Atlantic-Pacific moisture flux adjustment. We do not rule out the possibility that a full investigation of PLASIM-GENIE parametric uncertainty could generate a plausible ocean circulation without a flux adjustment, and may

additionally resolve the understated southern sea ice. However, a comprehensive tuning will demand the application of more complex statistical approaches designed to deal with computationally demanding simulators. For instance, the use of emulators to inform a sequential ensemble design process has been demonstrated to yield a ~100-fold reduction in computational demand (Holden et al 2015).

7.0 Code availability

The code base is stored on a password-protected SVN server

https://svn.ggy.bris.ac.uk/subversion/genie/branches/PLASIM_coupling

Contact the authors for the password. The model is under continuous development; see SVN revision 9657 for traceability.

We recommend setting up a root directory (e.g. PLASIM-GENIE) containing the subdirectories genie_output and genie, the latter containing the directory structure downloaded from the SVN repository.

In addition to the source code, PLASIM-GENIE makes use of several applications and packages. You must have the following list of prerequisites installed on your computer before you can run the model: Python, Perl, GNU make, the BASH shell, a C++ compiler, a Fortran compiler that supports Fortran90, and NetCDF libraries (compiled on the same computer using the same compilers that you will use to compile PLASIM-GENIE).

Before you compile the model you must provide information about i) where you have installed the source code, ii) which compilers you are using, and iii) the location of the netCDF libraries that you have created; this is achieved by editing the files **user.mak** and **user.sh** in the directory genie-main. Comments in those files explain which lines need to be edited.

A configuration file contains all the information required to specify a simulation. The code base includes a configuration file to perform a 1,000-year spin-up with the

subjective parameter set "genie/genie-main/configs/pl_go_gs_GMD.xml". This configuration file has been fully commented for traceability to this model description paper and to explain how to generalize to other model realisations. To run this simulation, enter the genie/genie-main directory and type:

```
make cleanall
./genie.job –f configs/pl_go_gs_GMD.xml
```

The outputs of this simulation will be directed to genie_output/GMD_subjective.

Acknowledgements. The work of Kirk, Lunkeit and Zhu was supported through the Cluster of Excellence 'CliSAP' (EXC177), Universität Hamburg, funded through the German Science Foundation (DFG).

References

Annan, J.D., Lunt D.J., Hargreaves, J.C. and Valdes, P.J.: Parameter estimation in an atmospheric GCM using the Ensemble Kalman Filter. Nonlinear Processes in Geophysics, European Geosciences Union (EGU), 12, 363-371, doi:1607-7946/npg/2005- 12-363, 2005.

Balan-Sarojini, B., Gregory, J. M., Tailleux, R., Bigg, G. R., Blaker, A. T., Cameron, D. R., Edwards, N. R., Megann, A. P., Shaffrey, L. C. and Sinha, B.: High frequency variability of the Atlantic meridional overturning circulation, Ocean Sci., 7, 471–486, doi:10.5194/os-7-471-2011, 2011.

Betts, A.K. and Miller, M.J.: A new convective adjustment scheme. Part II: Single column tests using GATE wave, BOMEX, ATEX and arctic air-mass data sets. Quart. J. R. Met. Soc., 112, 693–709, 1986.

Bondeau, A., Smith, P. C., Zaehle, S., Schaphoff, S., Lucht, W., Cramer, W., Gerten, D., Lotze-Campen, H., Müller, C., Reichstein, M., and Smith, B.: Modelling the role

of agriculture for the 20th century global terrestrial carbon balance, Glob. Change Biol., 13, 679–706, doi:10.1111/j.1365- 2486.2006.01305.x, 2007.

Budyko, M. : Climate and Life. Vol. 18, Academic Press, 508 pp, 1974.

Cai, D., Fraedrich, K., Sielmann, F., Guan, Y., Guo, S., Zhang, L. and Zhu, X.: Climate and vegetation: an ERA-interim and GIMMS NVDI analysis, Journal of Climate, 27, 5111-5118, doi: 10.1175/JCLI-D-13-00674.1, 2014

Cavalieri, D. J., Parkinson, C. L., and Yinnikov, K. Y.: 30-year satellite record reveals contrasting Arctic and Antarctic decadal sea-ice variability, Geophys. Res. Lett., 30, 1970, doi:10.1029/2003GL018031, 2003.

Dahms, E., Borth, H., Lunkeit, F., and Fraedrich, K.: ITCZ splitting and the influence of large-scale eddy fields on the Tropical mean state, J. Meteorol. Soc. Jpn., 89, 399–411, doi:10.2151/jmsj.2011-501, 2011.

Edwards, N.R. and Marsh, R.: Uncertainties due to transport-parameter sensitivity in an efficient 3-D ocean-climate model, Climate Dynamics, 24, 415-433, doi: 10.1007/s00382-004-0508-8, 2005.

Edwards, N.R., Willmott, A.J. and Killworth, P.D.:. On the role of topography and wind stress on the stability of the thermohaline circulation. J. Physical Oceanography, 28, 756-778, 1998.

Fanning, A. F. and Weaver, A. J.: An atmospheric energy-moisture balance model: climatology, interpentadal climate change, and coupling to an ocean general circulation model, Journal of Geophysical Research, 101, 15111–15128, doi:10.1029/96JD01017, 1996.

de Forster, P.M., Blackburn, M., Glover, R. and Shine, K.P.: An examination of climate sensitivity for idealised climate change experiments in an intermediate

759 general circulation model. Climate Dynamics, 16, 833–849, doi:
760 10.1007/s003820000083, 2000.
761
762 Fraedrich, K., Kirk, E., Luksch, U. and Lunkeit, F.: The portable university model of
763 the atmosphere (PUMA): Storm track dynamics and low-frequency variability,
764 Meteorologische Zeitschrift, 14, 735-745, doi: 10.1127/0941-2948/2005/0074, 2005.
765
766 Fraedrich, K. and Lunkeit, F.: Diagnosing the entropy budget of a climate model,
767 Tellus A, 60, 921–931, doi:10.1111/j.1600- 0870.2008.00338.x, 2008, 2008.
768
769 Fraedrich, K.: A suite of user-friendly climate models: Hysteresis experiments,
770 The European Physical Journal Plus, 127, 10.1140/epjp/i2012-12053-7, 2012
771
772 Fraedrich, K., Sielmann, F., Cai, D., and Zhu, X.: Climate dynamics on watershed
773 scale: along the rainfall-runoff chain. In: The Fluid Dynamics of Climate,
774 International Centre for Mechanical Sciences (CISM), Springer Verlag, 183-209,
775 2016.
776
777 Frierson, D.M.W., Held, I.M. and Zurita-Gotor, P.: A gray-radiation aquaplanet
778 moist GCM. Part I. Static stability and eddy scale, J. Atmos. Sci., 63, 2548-2566,
779 2006
780
781 Held, I.M. and Phillipps, P.J.: Sensitivity of the eddy momentum flux to meridional
782 resolution in atmospheric GCMs, Journal of Climate, 6, 499-507, 1995.
783
784 Hibler W.D.: Dynamic thermodynamic sea ice model, J Phys Oceanogr, 9, 815–
785 846, 1979.
786
787 Holden, P.B. and Edwards, N.R.: Dimensionally reduced emulation of an AOGCM
788 for application to integrated assessment modelling, Geophysical Research
789 Letters, 37, L21707, doi:10.1029/2010GL045137, 2010.
790

Holden, P.B., Edwards, N.R., Oliver, K.I.C, Lenton, T.M. and Wilkinson R.D.: A probabilistic calibration of climate sensitivity and terrestrial carbon storage in GENIE-1, Climate Dynamics, 35, 785-908, doi: 10.1007/s00382-009-0630-8, 2010.

Holden, P.B., Edwards, N.R., Gerten, D. and Schaphoff, S.: A model-based constraint on CO_2 fertilisation, Biogeosciences, 10, 339-355, doi:10.5194/bg-10-339-2013, 2013a.

Holden, P.B., Edwards, N.R., Müller, S.A., Oliver, K.I.C., Death, R.M. and Ridgwell, A.: Controls on the spatial distribution of $\delta^{13}C$, Biogeosciences, 10, 1815-1833, doi:10.5194/bg-10-1815-2013, 2013b.

Holden, P.B., Edwards, N.R., Garthwaite, P.H., Fraedrich, K., Lunkeit, F., Kirk, E., Labriet, M., Kanudia, A. and Babonneau, F.: PLASIM-ENTSem v1.0: a spatio-temporal emulator of future climate change for impacts assessment, Geosci. Model Dev., 7, 433–451, doi:10.5194/gmd-7-433-2014, 2014.

Holden, P.B., Edwards, N.R., Hensman, J. and Wilkinson, R.D.: ABC for climate: dealing with expensive simulators, In S. A. Sisson, Y. Fan, and M. Beaumont eds. Approximate Bayesian Computation: Likelihood-Free Methods for Complex Models, Chapman and Hall, in press.

Hoskins, B.J. and Simmons, A.J.: A multi-layer spectral model and the semi-implicit method, Quart. J. R. Met. Soc., 101, 637-655, doi: 10.1002/ qj.49710142918, 1975.

Kalnay, E., Kanamitsu, M., Kistler, R., Collins, W., Deaven, D., Gandin, L., Iredell, M., Saha, S., White, G., Woollen, J., Zhu, Y., Leetmaa, A., Reynolds, R., Chelliah, M., Ebisuzaki, W., Higgins, W., Janowiak, J., Mo, K. C., Ropelewski, C., Wang, J., Jenne, R., and Joseph, D.: The NCEP/NCAR 40-Year Reanalysis Project. Bull. Amer. Meteor. Soc., **77**, 437–471, 1996.

824 Labriet, M., Joshi, S.R., Vielle, M., Holden, P.B., Edwards, N.R., Kanudia, A.,
825 Loulou, R. and Babonneau, F.: Worldwide impacts of climate change on energy for
826 heating and cooling, Mitigation and Adaptation Strategies for Global Change, doi:
827 10.1007/s11027-013-9522-7, 2013.
828
829 Lenton, T.M., Williamson, M.S., Edwards, N.R., Marsh, R., Price, A.R., Ridgwell, A.J.,
830 Shepherd, J.G., Cox, S.J. and The GENIE team: Millennial timescale carbon cycle
831 and climate change in an Efficient Earth system model, Climate Dynamics, 26,
832 687-711, doi: 10.1007/s00382-006-0109-9, 2006.
833
834 Lenton, T. M., Aksenov, Y., Cox, S.J., Hargreaves, J.C., Marsh, R., Price, A.R., Lunt,
835 D.J., Annan, J.D., Cooper-Chadwick, T., Edwards, N.R., S. Goswami, S., Livina,
836 V.N., P. J. Valdes, P.J., Yool, A., Harris, P.P., Jiao, Z., Payne, A.J., Rutt, I.C.,
837 Shepherd, J.G. Williams, G., Williamson, M.S.: Effects of atmospheric dynamics and
838 ocean resolution on bi-stability of the thermohaline circulation examined using the
839 Grid Enabled Integrated Earth system modelling (GENIE) framework, Climate
840 Dynamics, 29, 591–613, doi:10.1007/s00382-007-0254-9, 2007.
841
842 Lunkeit, F., Böttinger, M., Fraedrich, K., Jansen, H., Kirk, E., Kleidon, A. and Luksch
843 U.: Planet Simulator Reference Manual Version 15.0,
844 http://epic.awi.de/29588/1/Lun2007d.pdf, 2007.
845
846 Kleidon, A., Fraedrich, K., and Low, C.: Multiple steady-states in the terrestrial
847 atmosphere-biosphere system: a result of a discrete vegetation classification?,
848 Biogeosciences, 4, 707–714, doi:10.5194/bg-4-707-2007, 2007.
849
850 Kuo, H. L.: On formation and intensification of tropical cyclones through latent heat
851 release by cumulus convection. J. Atmos. Sci., 22, 40–63, 1965.
852
853 Kuo, H. L.: Further studies of the parameterization of the influence of cumulus
854 convection on large-scale flow. J. Atmos. Sci., 31, 1232–1240, 1974.
855

Marsh, R., Müller, S.A., Yool, A. and Edwards, N.R.: Incorporation of the C-GOLDSTEIN efficient climate model into the GENIE framework: "eb-go-gs" configurations of GENIE, Geosci. Model Dev., 4, 957-992, doi:10.5194/gmd-4-957-2011, 2011.

Matthews, H.D. and Caldeira, K.: Transient climate-carbon simulations of planetary geoengineering, PNAS, 104, 9949–9954, doi:10.1073/pnas.0700419104, 2007.

Mercure, J.-F., Pollitt, H., Chewpreecha, U., Salas, P., Foley, A.M., Holden, P.B. and Edwards, N.R.: The dynamics of technology diffusion and the impacts of climate policy instruments in the decarbonisation of the global electricity sector, Energy Policy, 73, 686-700, doi:10.1016/j.enpol.2014.06.029, 2014.

Micheels, A. and Montenari, M.: A snowball Earth versus a slush-ball Earth: Results from Neoproterozoic climate modeling sensitivity experiments, Geosphere, 4, 401–410, doi: 10.1130/GES00098.1, 2008.

Molteni, F.: Atmospheric simulations using a GCM with simplified physical parameterizations. I: Model climatology and variability in multi-decadal experiments, Climate Dynamics, 20, 175–191, 2003.

Oliver, K. I. C. and Edwards, N. R.: Location of potential energy sources and the export of dense water from the Atlantic Ocean, Geophys. Res. Lett., 35, L22604, doi:10.1029/2008GL035537, 2008.

Oort, A.H.: Global atmospheric circulation statistics, 1958– 1973:NOAA Prof Pap 14, 1983.

Pacanowski, R.: MOM 2 Documentation User's Guide and Reference Manual, GFDL Ocean Group Technical Report. NOAA, GFDL. Princeton, 232pp, 1995.

Plattner, G.-K., R. Knutti, F. Joos, T. F. Stocker, W. von Bloh, V. Brovkin, D. Cameron, E. Driesschaert, S. Dutkiewicz, M. Eby, N. R. Edwards, T. Fichefet, J. C.

889 Hargreaves, C. D. Jones, M. F. Loutre, H. D. Matthews, A. Mouchet, S. A. Mueller, S.
890 Nawrath, A. Price, A. Sokolov, K. M. Strassmann, and A. J. Weaver 2008 Long-term
891 climate commitments projected with climate - carbon cycle models. Journal of
892 Climate, Vol. 21, pp. 2721-2751, doi: 10.1175/2007JCLI1905.1, 2008
893
894 Roscher, M., Stordal, F., and Svenson, H.: The effect of global warming and global
895 cooling on the distribution of the latest Permian climate zones, Palaeogeogr.
896 Palaeocl., 309, 186–200, doi:10.1016/.j.palaeo.2011.05.042, 2011.
897
898 Sarojini, B.B., Gregory, J.M., Tailleuc, R., Bigg, G.R., Blaker, A.T., Cameron, D.R.,
899 Edwards, N.R., Megann, A.P., Shaffrey, L.C. and Sinha, B.: High frequency
900 variability of the Atlantic meridional overturning circulation, Ocean Science, 7, 471-
901 486, doi:10.5194/os-7-471-2011, 2011.
902
903 Schmittner, A., Silva, T.A.M., Fraedrich, K., Kirk, E. and Lunkeit, F.: Effects of
904 mountains and ice sheets on global ocean circulation, Journal of Climate, 24, 2814-
905 2829, DOI: 10.1175/2010JCLI3982.1, 2010.
906
907 Semtner, A.J.: Model for thermodynamic growth of sea ice in numerical
908 investigations of climate, J Phys Oceanogr, 6, 379–389, 1976.
909
910 Severijns, C.A. and Hazeleger, W.: The efficient global primitive equation climate
911 model SPEEDO V2.0, Geosci. Model Dev., 3, 105-122, www.geosci-model-
912 dev.net/3/105.2010/, 2010.
913
914 Slingo, A., and Slingo, J.M.: Response of the National Center for Atmospheric
915 Research community climate model to improvements in the representation of clouds.
916 J. Geoph. Res., 96, 341-357, 1991.
917
918 Talley, L.D.: Freshwater transport estimates and the global overturning circulation:
919 Shallow, deep and throughflow components, Progress in Oceanography, 78, 257-303,
920 doi:10.1016/j.pocean.2008.05.001, 2008.
921

Trenberth, K.E., Smith, L., Qian, T., Dai, A. and Fasullo, J.: Estimates of the global water budget and its annual cycle using observational and model data, Journal of Hydrometeorology – Special Section, 8, 758-769, doi: 10.1175/JHM600.1, 2007.

Trenberth, K.E., Fasullo, J.T. and Kiehl, J.: Earth's global energy budget, Bulletin of the American Meteorological society, 90, 311-323, doi:10.1175/2008BAMS2634.1, 2009.

Williams, J.H.T., Smith, R.S., Valdes, P.J., Booth, B.B.B. and Osprey, A.: Optimising the FAMOUS climate model: inclusion of global carbon cycling, Geosci. Model Dev., 6, 141-160, doi: 10.5194/gmd-6-141-2013, 2013.

Williamson, D., Blaker, A.T., Hampton, C. and Salter, J.: Identifying and removing structural biases in climate models with history matching, Climate Dynamics, 45, 1299-1324, doi: 10.1007/s00382-014-2378-z, 2015.

Williamson, M.S., Lenton, T.M., Shepherd, J.G. and Edwards, N.R.: An efficient numerical terrestrial scheme (ENTS) for Earth system modelling, Ecological modelling, 198, 362-374, doi:10.1016/j.ecolmodel.2006.05.027, 2006.

Zickfeld, K., Eby, M., Weaver, A. J., Crespin, E., Fichefet, T., Goosse, H., Philippon-Berthier, G., Edwards, N. R., Holden, P. B., Eliseev, A. V., Mokhov, I. I., Feulner, G., Kienert, H., Perrette, M., Schneider von Deimling, T., Forest, C. E., Joos, F., Spahni, R., Steinacher, M., Kawamiya, M., Tachiiri, K., Kicklighter, D., Monier, E., Schlosser, A., Sokolov, A. P., Matsumoto, K., Tokos, K., Olsen, S. M., Pedersen, J. O. P., Shaffer, G., Ridgwell, A., Zeng, N., and Zhao, F.: Long-term climate change commitment and reversibility, J. Climate, 26, 5782-5809, doi: 10.1175/JCLI-D-12-00584.1, 2013.

TABLES

Parameter	Description	Range	Subjective tuning
APM (Sv)	Atlantic-Pacific moisture flux adjustment	0 to 0.32	0.2132
OVD (m^2s^{-1})	Reference diapycnal diffusivity	$2x10^{-5}$ to $2x10^{-4}$	$1.583x10^{-4}$
OHD (m^2s^{-1})	Isopycnal diffusivity	500 to 5,000	1,937
SCF (dimensionless)	Wind stress scaling	2 to 4	3.788
ADRAG (days)	Inverse ocean drag	0.5 to 5.0	2.069
OP1 (dimensionless)	Power law for diapycnal diffusivity depth profile	0.5 to 1.5	0.8200

***Table 1**: Ensemble varied parameters.*

Solar radiation (Wm^{-2})					
	Incoming TOA	Reflected by atmosphere	Absorbed by atmosphere	Reflected by surface	Absorbed by surface
PLASIM-GENIE	341	75	66	39	161
ERBE (1985-1989)	339-343	70-83	64-81	23-45	156-169
CERES (2000-2004)	339-342	69-82	64-78	23-45	161-170
Planetary radiation and heat fluxes (Wm^{-2})					
	Sensible heat	Latent heat	Back radiation	Upward surface radiation	Outgoing radiation OLR
PLASIM-GENIE	20	78	323	386	228
ERBE (1985-1989)	15-24	78-85	324-345	390-396	235-254
CERES (2000-2004)	15-19	83-90	324-345	394-397	236-254

Table 2: *The global energy balance of subjectively-tuned PLASIM-GENIE in the preindustrial state compared against estimates derived from the 'Earth Radiation Budget Experiment' ERBE (1985-1989), when the Earth's radiation balance was in approximate equilibrium, and the 'Clouds and Earth's Radiant Energy System' CERES data (2000-2004). The observational uncertainties reflect a range of analyses summarised in Trenberth et al (2009).*

Surface ocean moisture fluxes (Sv)						
	Atlantic/Arctic Ocean	Pacific Ocean	Indian Ocean	Southern Ocean	Total Ocean	Trenberth et al (2007)
Precipitation	1.96	4.76	1.67	2.89	**11.28**	11.8
Evaporation	-2.68	-5.48	-1.98	-2.52	**-12.66**	-13.1
Run off	0.59	0.36	0.23	0.18	**1.37**	1.3
Flux adjustment	-0.21	0.21	0.00	0.00	**0.00**	
Net	**-0.34**	**-0.14**	**-0.07**	**0.56**	**0.00**	
Talley (2008)	-0.28±0.04	0.04±0.09	-0.37±0.10	0.61±0.13		

Table 3: *Simulated surface ocean moisture fluxes of the subjective tuning and observationally constrained estimates. The definition of ocean basin boundaries follows Talley (2008) viz. Atlantic and Indian Oceans north of 32°S, Pacific Ocean north of 28°S.*

964 **FIGURES**

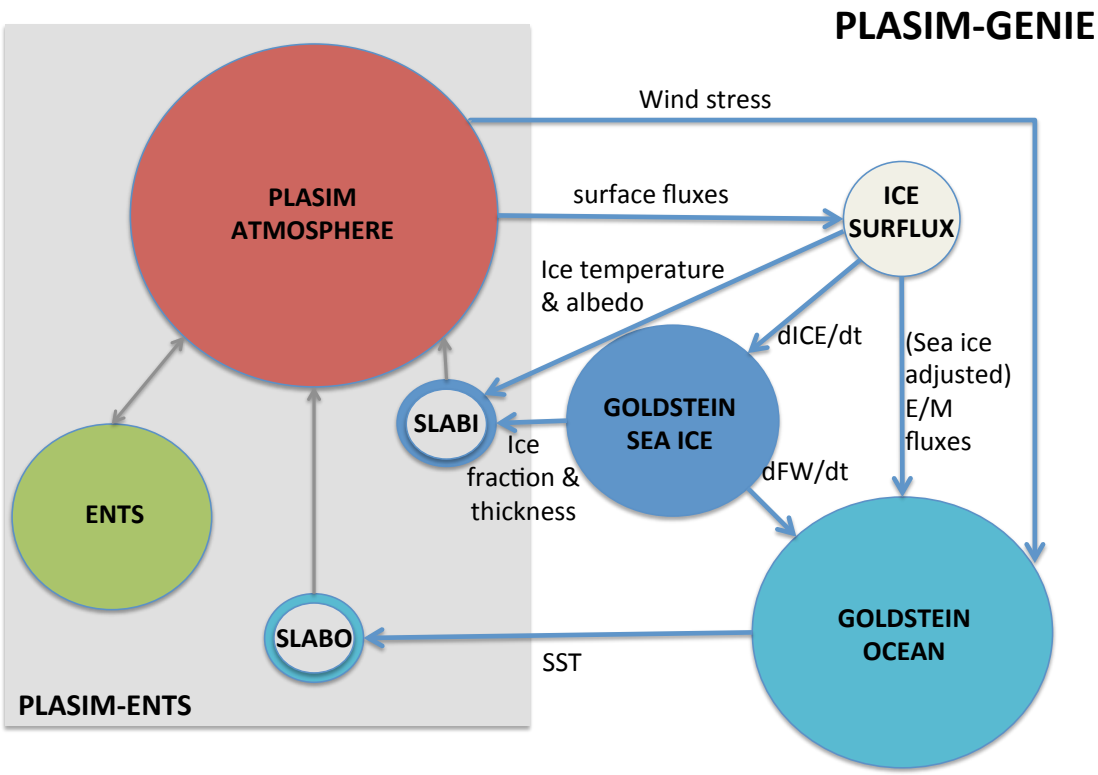

965
966
967 **Figure 1**: A schematic of the PLASIM-GENIE coupling. The circles represent the
968 component modules, with sizes indicative of their relative complexity. The grey
969 box defines the PLASIM-ENTS model, which has been retained in its entirety;
970 hollow circles (SLABO and SLABI) are dummy PLASIM modules, retained only to
971 specify ocean and sea-ice boundary conditions from GOLDSTEIN outputs; grey
972 lines are energy and moisture fluxes that are calculated within the pre-existing
973 PLASIM-ENTS coupling. Blue arrows are variables passed in the PLASIM-GENIE
974 coupling. ICE-SURFLUX is the new surface flux routine that was developed for
975 the coupling (see Section 3.3)
976

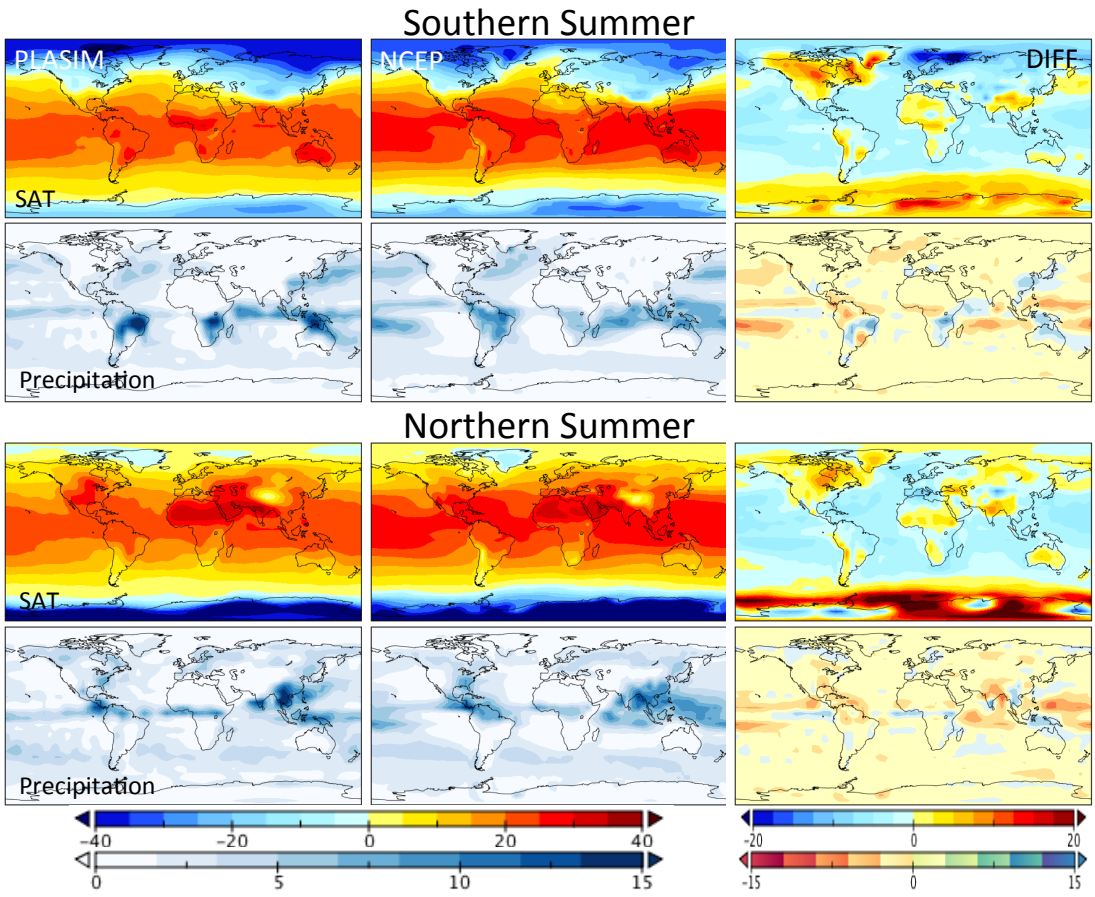

977
978 **Figure 2**: Seasonal surface air temperature (°C) and precipitation (mm/day).
979 Left: PLASIM-GENIE 50-year average. Centre: long-term average (1981-2010)
980 NCEP/NCAR reanalysis fields (Kalnay et al 1996). Right: difference (PLASIM-
981 NCEP).
982

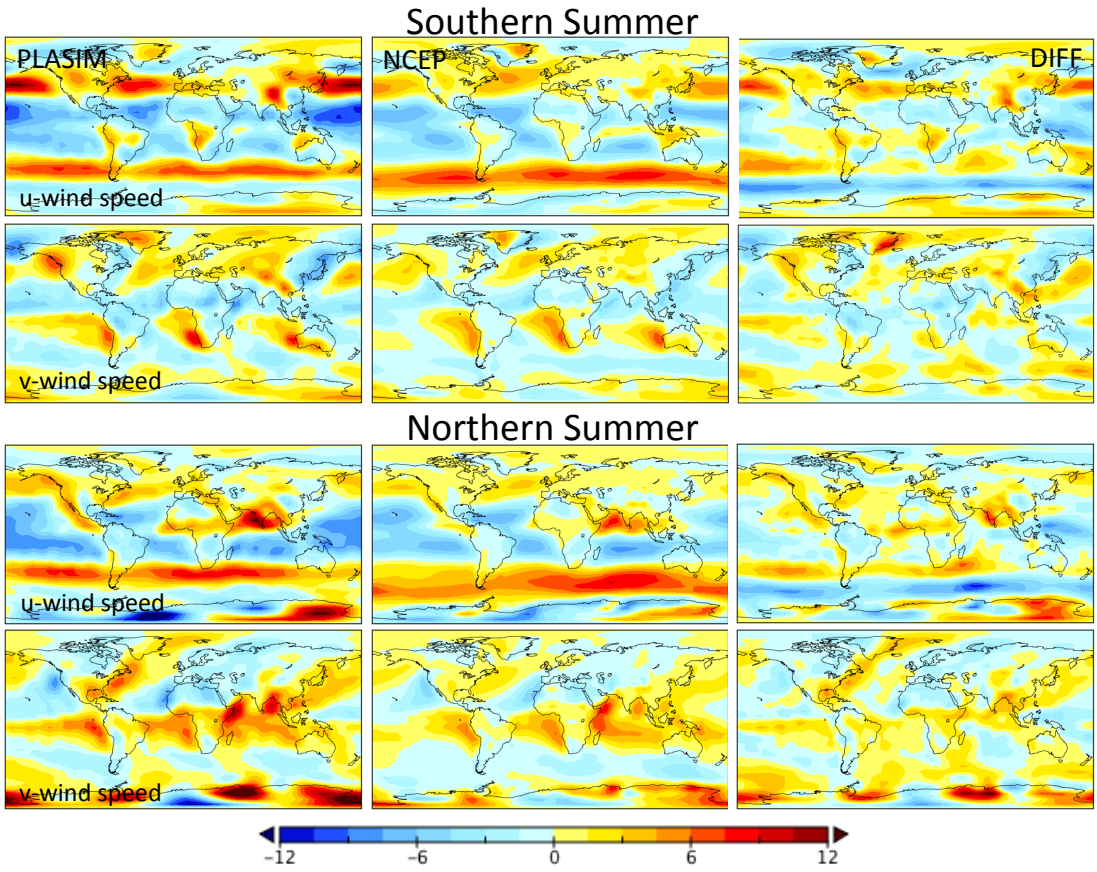

Figure 3: Seasonal surface zonal and meridional wind speeds (ms^{-1}). Left: PLASIM-GENIE 50-year average. Centre: long-term average (1981-2010) NCEP/NCAR reanalysis fields (Kalnay et al 1996). Right: difference (PLASIM-NCEP).

990

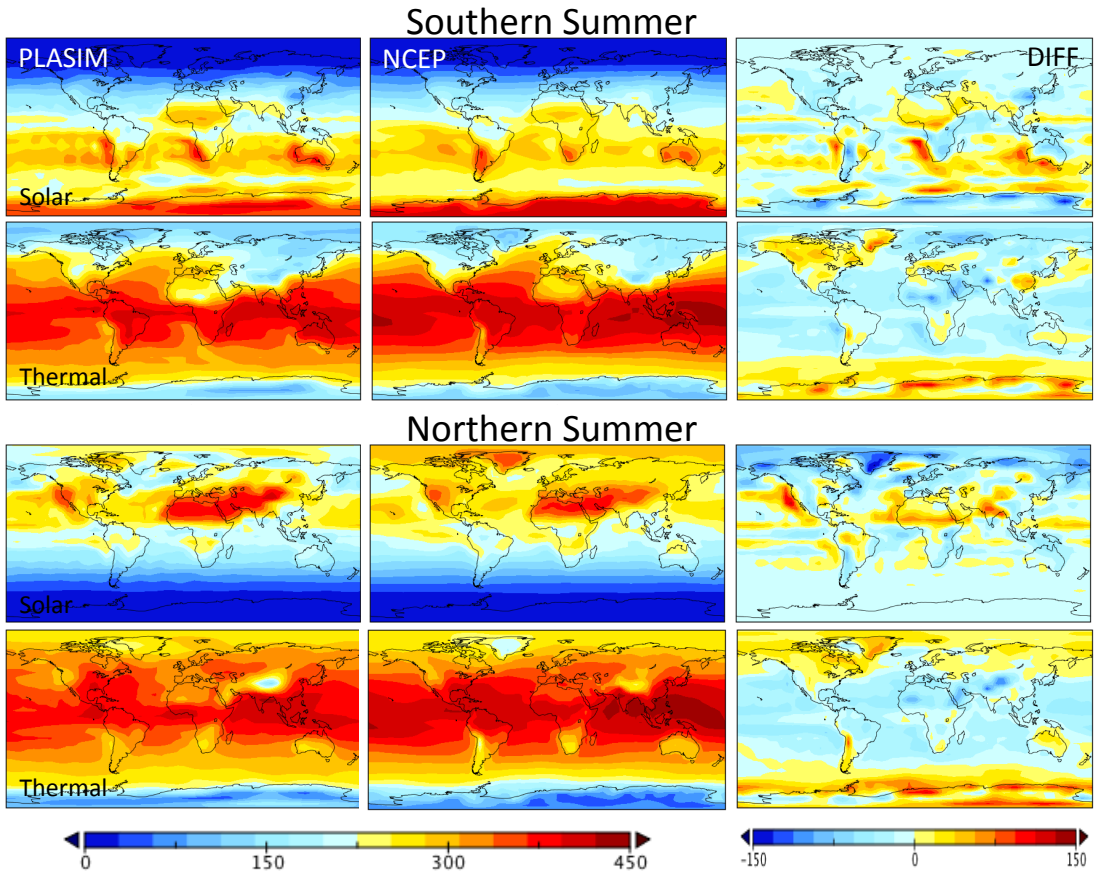

991
992

993 **Figure 4**: Seasonal incoming surface solar and thermal radiation (Wm^{-2}). Left:
994 PLASIM-GENIE 50-year averages. Centre: long-term average (1981-2010)
995 NCEP/NCAR reanalysis fields (Kalnay et al 1996). Right: difference (PLASIM-
996 NCEP).

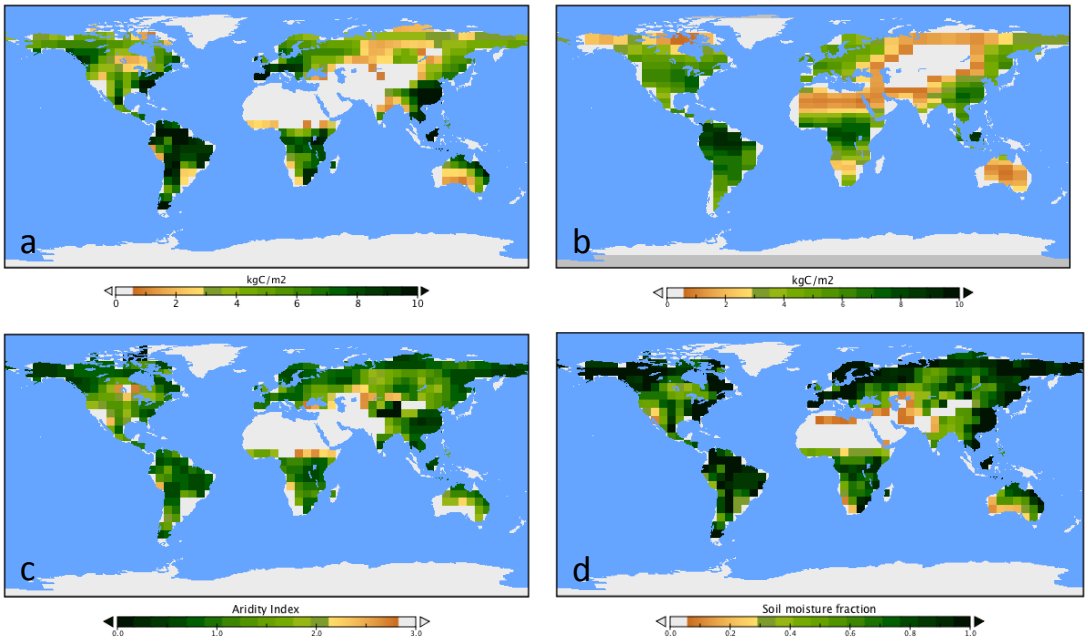

Figure 5: Land surface. a) ENTS vegetation carbon density from PLASIM-GENIE, b) ENTS vegetation carbon density from GENIE-1 (Holden et al 2013a), c) Budyko aridity index N/P and d) soil moisture fraction E/N

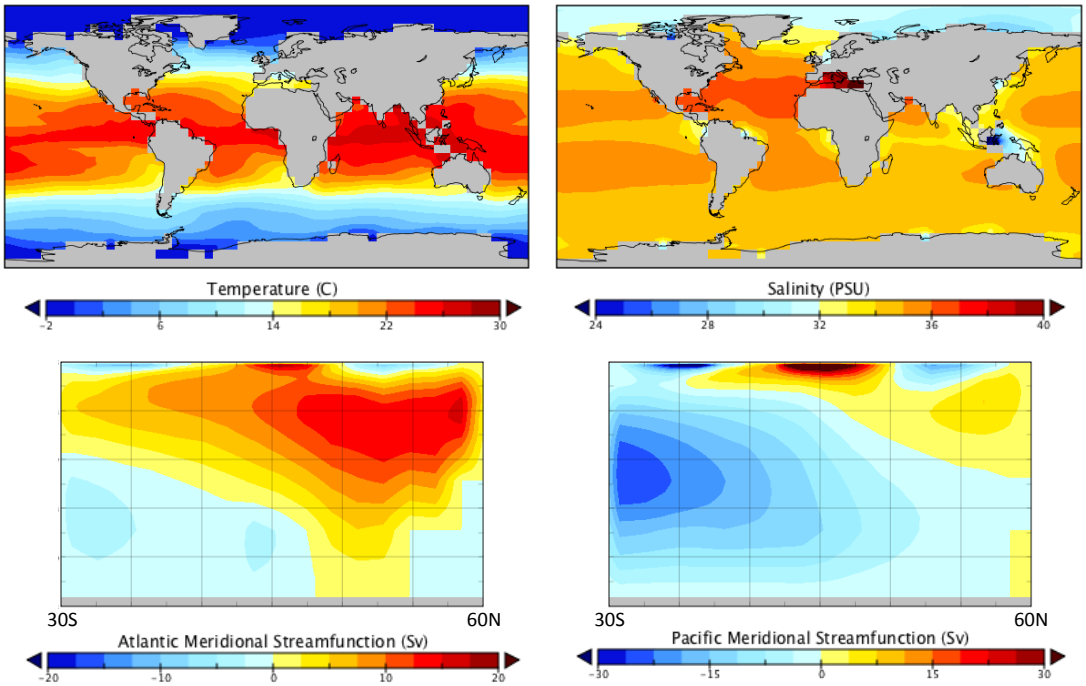

Figure 6: Ocean. Upper panels: PLASIM-GENIE simulated surface ocean temperature and salinity. Lower panels: PLASIM-GENIE simulated Atlantic and Pacific meridional stream functions.

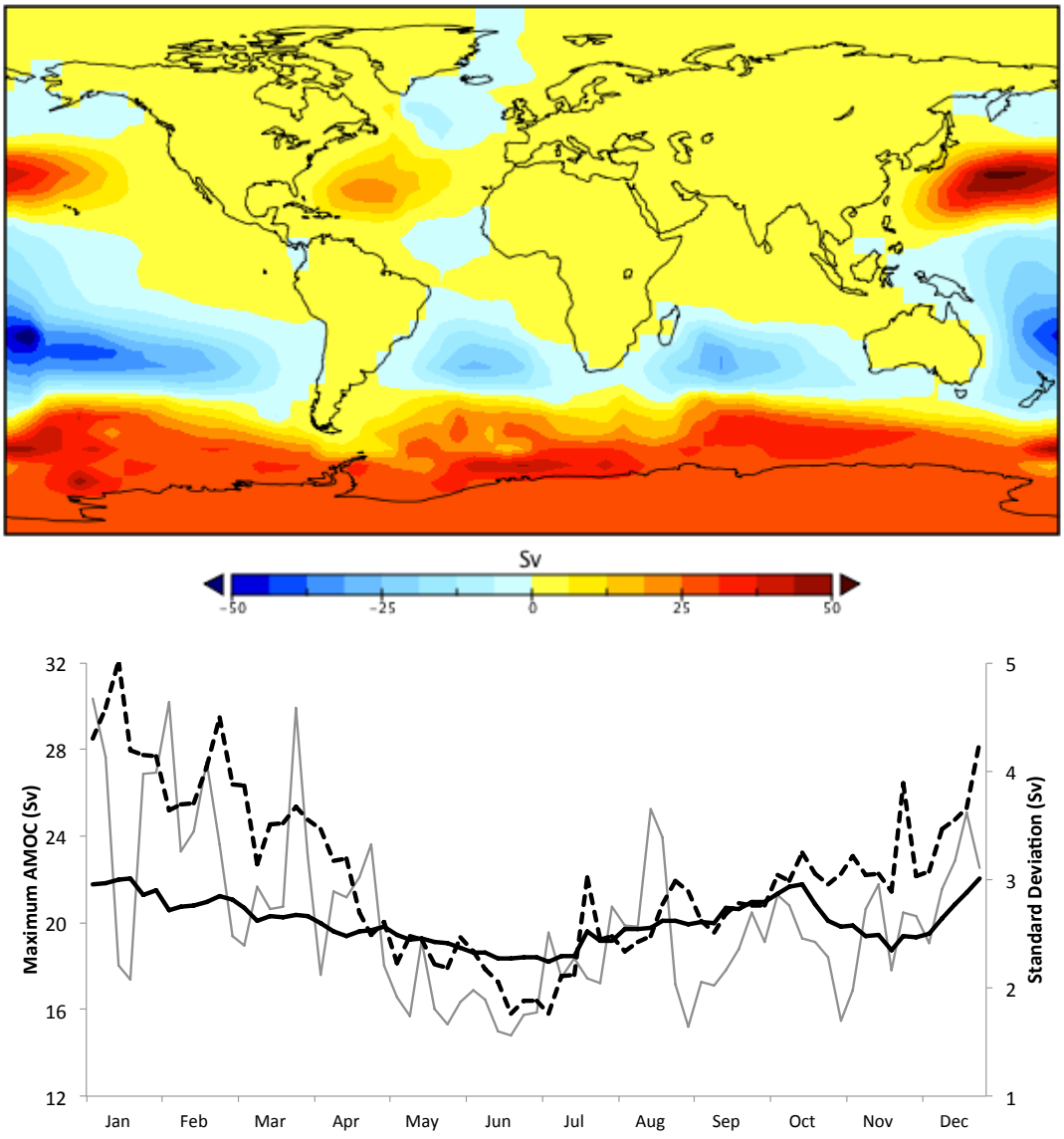

Figure 7: Upper panel: PLASIM-GENIE barotropic stream function. Lower panel: Wind-driven AMOC variability: solid black 100-year mean, dashed black 100-year standard deviation, solid grey arbitrary year (year 100 of a spin-on simulation)